Applied Surface Science 620 (2023) 156786

Contents lists available at ScienceDirect

Applied Surface Science

journal homepage: www.elsevier.com/locate/apsusc

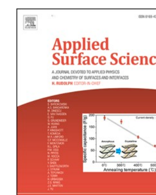

Full Length Article

Highly efficient and atomic scale polishing of GaN via plasma-based atom-selective etching

Linfeng Zhang, Bing Wu, Yi Zhang, Hui Deng *

Department of Mechanical and Energy Engineering, Southern University of Science and Technology, No. 1088, Xueyuan Road, Shenzhen, Guangdong 518055, China

ARTICLE INFO

Keywords:
PASE
Subsurface damage
Surface roughness
GaN
Plasma etching

ABSTRACT

Plasma-based atom-selective etching (PASE) of GaN is conducted to realize the highly efficient planarization of the GaN surface. Inductively coupled plasma with high temperature and high concentration of radicals is used as the source of PASE. The non-toxic carbon tetrafluoride is chosen over chlorine as the reaction gas, and the volatility of the etching products will be improved at high temperatures in the PASE of GaN. After 2 min of PASE, the GaN surface roughness is reduced from *Sa* 135.8 nm to *Sa* 0.527 nm. The material removal rate of PASE of GaN is measured to be 93.01 μm/min, thousands of times higher than that of the conventional chemical mechanical polishing method. The crystal structure of the GaN subsurface is well-ordered without any damage or defects. PASE is thus proven to be a non-destructive etching method. In this study, the effects of radio frequency power and reaction gas flow rate on PASE are also investigated. Surface temperature and concentration of radicals are found to be the critical factors in the PASE of GaN.

1. Introduction

GaN is a promising semiconductor material with excellent chemical and electrical properties. It has a wide range of applications in high electron mobility transistor (HEMT) and light emitting diode (LED) fields [1,2]. To achieve better performance of GaN-based devices, an ultra-smooth surface free of scratches and subsurface damage is required. After the crystal growth process, grinding and lapping are conducted to correct the wafer thickness. Due to the high brittleness of GaN, conventional mechanical polishing (MP) using hard abrasives will inevitably induce scratches and subsurface damage, which is detrimental to further device fabrication. Chemical mechanical polishing (CMP) is currently the most widely used GaN planarization technique. Scratches and subsurface damage introduced by the preceding process can be completely removed by CMP. Due to the chemical inertness of GaN, it takes at least 8 h of CMP to remove the subsurface damage [3]. Recently, great efforts have been made to improve the surface roughness and material removal rate (MRR) of CMP by applying an external energy field and adding catalysts [4–6]. The MRR can reach up to around 250 nm/h through the above methods, however, it still cannot meet the needs of emerging applications.

Many studies have been carried out to improve the MRR and surface flatness of GaN. As a wet etching technique, catalyst-referred etching (CARE) utilizes a catalyst plate placed against the GaN wafer and neutral buffer solution to generate reactive species. The GaN wafer rotates relatively to the polishing plate under a controlled load and is flattened through chemical reactions. Surface roughness of 0.1 nm rms can be achieved through CARE, while the MRR is only 4 nm/h [7]. With the aid of the Photoelectrochemical (PEC) reaction, the MRR of CARE can reach 800 nm/h, but the roughness will deteriorate to 0.520 nm rms simultaneously [8]. Photoelectrochemically combined mechanical polishing (PECMP) was developed for the finishing of the *N*-type GaN surface. The GaN wafer surface is exposed to ultraviolet illumination and oxidized, and the oxide layer is mechanically polished subsequently. Through PECMP, the GaN surface roughness can be reduced to *Sa* 0.21 nm, and the MRR can reach 275.3 nm/h [9,10].

Due to the chemical inertness of GaN, wet etching based on the use of electrolytes can not significantly improve the MRR. In surface planarization techniques utilizing abrasives, the improvement of MRR is often accompanied by the deterioration of surface roughness. In addition, the use of electrolytes is environmentally harmful and requires expensive post-treatment processes. As a dry etching technique, plasma etching has been widely used in the fabrication of electronic devices [11,12]. Low-pressure plasma etching containing high-energy ions will induce defects and subsurface damage on the surface. Beyond that, the surface integrity after etching is poor due to preferential etching of dislocations

* Corresponding author.
E-mail address: dengh@sustech.edu.cn (H. Deng).

https://doi.org/10.1016/j.apsusc.2023.156786
Received 12 January 2023; Received in revised form 11 February 2023; Accepted 15 February 2023
Available online 18 February 2023
0169-4332/© 2023 Elsevier B.V. All rights reserved.

and defects [13–15].

The atmospheric plasma has a low mean free path, which avoids the introduction of damage and reduces the cost of using a high vacuum chamber [16,17]. Several kinds of atmospheric plasma-based etching techniques have been developed for the processing of hard-to-machine materials. Plasma chemical vaporization machining (PCVM) was first developed for chemical figuring and finishing for optical materials [18–20]. Material removal of PCVM is achieved through chemical reactions, rather than high-energy ion bombardment. Cl_2 and He are used as the reaction gases for the PCVM of GaN. The MRR of PCVM can reach 9100 nm/min, but it has no improvement in surface roughness [21]. Reactive atom plasma technology (RAPT) was developed by the US Lawrence Livermore National Laboratory (LLNL) and RAPT Inc (US) [22]. Atmospheric inductively coupled plasma is utilized in RAPT for the surface finishing of SiC and ultra-low expansion (ULE) glass [22,23]. RAPT can effectively remove the residual stress and damage induced by abrasive grinding and improve the surface form simultaneously. However, RAPT has no surface flattening effect as reported [24]. Plasma-assisted polishing (PAP) utilizes capacitively coupled plasma to irradiate the GaN surface and form a soft modified layer on the surface. Soft abrasives are used to remove the modified layer without inducing damage to the substrate. PAP is a non-destructive polishing method, and the surface roughness can be reduced to *Sq*0.08 nm. However, the MRR is only around 200 nm/h [25].

Conventional plasma etching of GaN mainly uses chlorine-based gases such as chlorine (Cl_2) and boron trichloride (BCl_3) [26–29]. Chlorine-based gas will generate Cl radicals during the ionization process, and its reaction products with GaN, $GaCl_3$, and NCl_3, have good volatility. However, chlorine is a hazardous gas, which is irritating to the eyes, respiratory tract, and mucous membranes. F-based plasmas such as carbon tetrafluoride (CF_4) plasma are commonly used for surface modification or treatment of GaN [25,30,31]. This is because its etching product GaF_3 has poor volatility at room temperature [21]. GaF_3 will be deposited on the surface, suppressing the etching reaction and deteriorating the surface roughness of GaN.

To achieve the highly efficient and non-destructive surface planarization of GaN, we propose a plasma-based atom-selective etching (PASE) method. PASE has been successfully applied to the surface polishing of silicon wafer, and an ultrasmooth surface without subsurface damage is achieved [32]. PASE utilizes a fully ionized atmospheric inductively coupled plasma, providing high temperature and high concentration of radicals. Surface planarization is realized through the selective removal of the step atoms which form the surface roughness. In this study, PASE is carried out to achieve the surface planarization of GaN. The mechanism of GaN surface planarization through PASE is proposed. The contribution of surface temperature to the realization of PASE is verified. Finally, the reasons for the surface roughness deterioration after PASE are discussed.

2. Experimental details

Unintentionally-doped freestanding GaN wafers supplied by Suzhou Nanowin Co. ltd. were used in this study. As-grown GaN samples and samples after lapping were used in different experiments. The dimension of the sample is 10×10 mm, with a dislocation density of 1×10^{-6} cm^{-2}. Before and after PASE, the samples were ultrasonically cleaned with absolute ethyl alcohol for 10 min to remove the contaminants, followed by rinsing with deionized water to remove residual alcohol.

Fig. 1(a) shows the schematics of the experimental setup of PASE. Among them, the inductively coupled plasma (ICP) torch is the most important component which is used for containing plasma. The optical image of ICP torch is shown in Fig. 1(b). The ICP torch consists of coaxial outer and inner tubes. Argon (Ar) gas is injected tangentially into the gap between the outer tube and the inner tube as a cooling gas. It descends through a spiral path to prevent the quartz torch from melting due to the high temperature of the plasma [33]. Argon also acts as a carrier gas and is injected into the inner tube along with the reaction gas CF_4. The flow rate of each gas is controlled by the corresponding mass

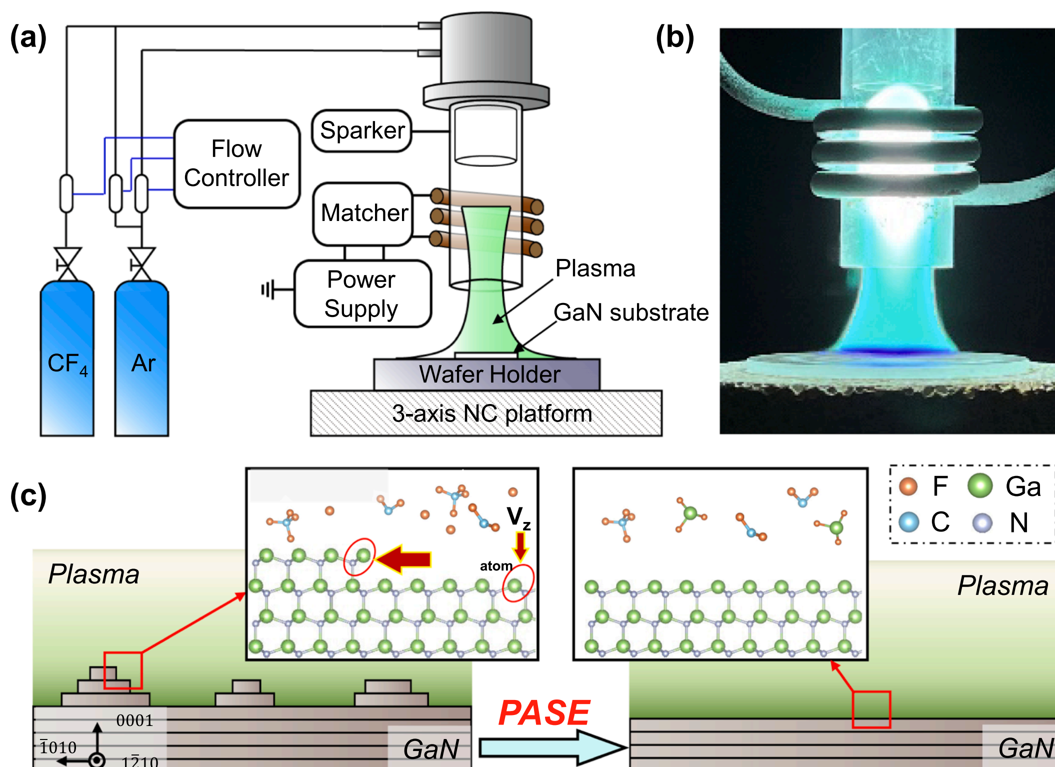

Fig. 1. (a) Schematic diagram of the experimental setup of PASE. (b) Optical image of the inductively coupled plasma torch. (c) Schematics of the mechanism of the PASE process.

flow controller. Three turns of copper coils are placed outside the outer tube, and both ends of the coils are connected to a radio frequency (RF) power supply. Circulating cooling water flows through the coils to prevent it from overheating and melting. A high-frequency alternating electric field is generated by an RF power supply in the plasma torch, which provides energy for the generation and maintenance of plasma. The sparker is used to pre-breakdown the carrier gas and generate free electrons, which are accelerated into high-energy electrons by the alternating electric field. An impedance matching system is utilized to eliminate reflected power from the circuit, allowing the energy to be fully coupled to the plasma [34].

The GaN surface temperature during PASE was measured using an infrared thermometer. The temperature values of the infrared thermometer were calibrated according to the emissivity of GaN. The temperature values shown in all results were the average temperature of the GaN surface. The radicals in the plasma could be identified and quantified by optical emission spectroscopy (OES). The peak intensities in the spectra were positively correlated to the relative concentration of the corresponding radicals in the plasma. The probe of the OES was fixed at a distance of approximately 100 mm from the center of the torch, and the integration time was 10 ms. During the experiment, the position of the plasma torch was fixed. The GaN wafer was placed on a piece of quartz holder, the position of which was controlled by a three-axis numerical control (NC) motion stage. The entire ICP equipment was placed inside an enclosure with a ventilation system to prevent possible toxic by-products of the reaction from leaking into the laboratory. The by-products generated during the PASE process were pumped to the exhaust pipe by a mechanical pump. After exhaust gas treatment, the by-products were discharged into the atmosphere.

Fig. 1(c) shows the mechanism of PASE. The rough GaN surface consists of many atom steps, where the atoms can be classified as the step edge (SE) atoms and the step terrace (ST) atoms. Due to the different bonding states of these atoms, the chemical activities of these atoms also show a discrepancy [35]. By tuning the operating parameters of plasma, the difference in reaction activity is magnified and the SE-atoms are prone to be removed from the surface. From a macroscopic view, the horizontal etching rate V_h can be fairly higher than the vertical etching rate V_z, which results in the surface planarization of GaN.

The operating parameters of PASE are shown in Table 1. The RF power and flow rate of reaction gas CF_4 were optimized, while other parameters were held constant in this study.

The composition of reactive radicals and their densities in the plasma were examined by optical emission spectroscopy (OES, Ocean optics USB4000). The chemical composition of the GaN surface before and after PASE was examined by X-ray photoelectron spectroscopy (XPS, Quantum 2000, ULVAC-PHI) with AlKα radiation (1486.6 eV). All peaks have been calibrated by C1s (284.8 eV) corresponding to carbon contaminations. The surface morphology was examined by scanning electron microscope (SEM, Zeiss Merlin). The temperature of the GaN surface during PASE was measured by an infrared thermal camera (FLIR T660). The surface roughness was measured through both scanning white light interferometry (SWLI, Taylor Hobson CCI) and atomic force microscope (AFM, Bruker Dimension Edge). The weight of the samples was measured by a precision balance (METTLER TOLEDO CC-3372–02). The subsurface crystal structure and surface elemental composition were detected by double-cs correction scanning transmission electron microscope (STEM, Titan themis G2) operated at an accelerating voltage of 300 kV. The TEM specimen was prepared by focused ion beam (FIB, Helios 600i).

Table 1
Operating parameters used in the PASE of GaN.

Parameters	Values
RF power	600 ~ 1000 W
RF frequency	27.12 MHz
Flow rate of cooling gas	Ar (18.0 slm)
Flow rate of reaction gas	CF_4 (0 ~ 60 sccm)
Flow rate of carrier gas	Ar (1.5 slm)
Work distance	15 mm

3. Results and discussion

3.1. Mechanism and decisive factors in PASE of GaN

With regards to the atmospheric radiofrequency ICP, the collision frequency of particles is low compared to the low-pressure plasma. The removal of material is mainly based on chemical reactions, and surface temperature and concentration of radicals will affect the etching characteristics. To optimize and verify the effect of operating parameters on the PASE of GaN, RF power and flow rate of reaction gas CF_4 were considered in this study. The RF power mainly affects the plasma temperature, and further affects the temperature of the sample surface. The flow rate of CF_4 mainly influences the concentration of reactive radicals in the plasma.

The concentration of radicals in plasma was evaluated by optical emission spectra (OES). Fig. 2(a) compares the OES of the Ar plasma with and without the addition of CF_4 gas. Only peaks corresponding to Ar-related species are detected by OES without adding the CF_4 gas. When CF_4 is added to the plasma, strong peaks corresponding to CF_x and C_2 radicals are detected. The peak located at 516.36 nm can be classified as the C_2 peak [36]. And the peak corresponding to 387.76 nm can be attributed to the CF_x peak [32]. C_2 radicals are formed during the dissociation of CF_4, whose intensity is positively correlated with the concentration of reactive F radicals. Fig. 2(b) summarizes the intensities of C_2 peaks under different RF powers. The intensity of the C_2 peak increases with the increase of RF power, indicating that high RF power promotes the dissociation process of CF_4. As the RF power increases, the plasma obtains more energy from the electric field, accelerating the dissociation rate of CF_4. As a result, the percentage of CF_4 molecules dissociated increases, which means that the plasma contains more F radicals.

Fig. 2(c) shows the intensities of the C_2 peak under different flow rates of CF_4. As the flow rate of CF_4 increases, the intensity of C_2 peaks also increases. When the supplied RF power is sufficient to completely ionize the CF_4 molecules, the dissociation degree of CF_4 molecule almost maintains constant under the same RF power. When the total number of CF_4 molecules increases, the concentration of F radicals in the plasma increases linearly. Since the ionization degree of the plasma is high enough, it is more effective to increase the CF_4 flow rate to increase the C_2 intensity.

The surface chemical compositions before and after PASE were investigated by X-ray photoelectron spectroscopy (XPS). The details of Ga3d spectra are summarized in Table 2. Fig. 3(a) shows the Ga3d and C1s XPS spectra of the as-grown GaN surface. The Ga3d spectra can be fitted with three components according to binding energy (BE): Ga-N (BE = 20.3 eV), Ga-O (BE = 21.1 eV), and metal Ga (BE = 17.6 eV) [37–39]. The C1s spectra can be fitted with only one component: C—C (BE = 284.8 eV). On the as-grown GaN surface, no obvious F-related peaks can be detected. Fig. 3(b) shows the Ga3d and C1s XPS spectra of the GaN surface after PASE with an RF power of 500 W. Different from the as-grown surface, the Ga-F peak (BE = 23.1 eV) and Ga…H-F (BE = 19.3 eV) peak are detected, and the peak corresponding to metal Ga disappears. The hydrogen may come from the dissociation of H_2O from the ambient. The C1s spectra can be fitted with three components: C—C, C—O (BE = 286.3 eV), and C-F (BE = 289.0 eV). Under this condition, the surface temperature is not sufficient for the reaction products to volatilize and escape from the surface. The etching products are deposited on the surface and inhibit the continuation of the reaction. Fig. 3(c) shows the Ga3d and C1s XPS spectra of the GaN surface after PASE with an RF power of 700 W. The Ga3d spectra can be fitted with three components: Ga-N, Ga-O, and metal Ga, which are identical to the

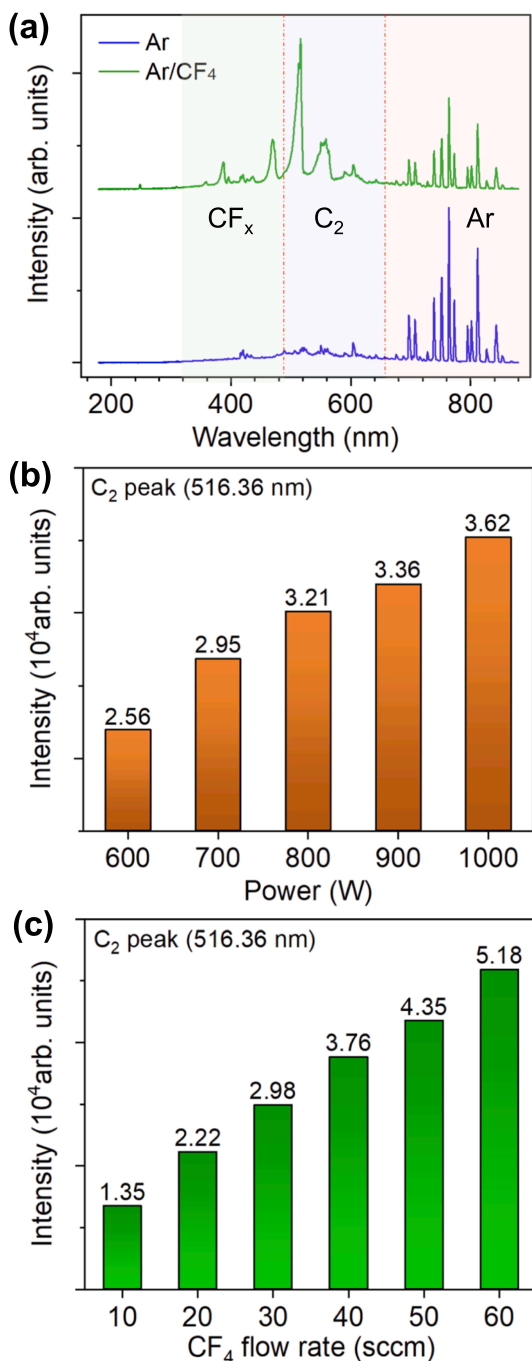

Fig. 2. (a) Optical emission spectra of Ar and Ar/CF_4 inductive coupled plasma; (b) Intensities of C_2 peak under different RF powers (CF_4 flow rate = 30 sccm); (c) Intensities of C_2 peak under different flow rates of CF_4 (RF power = 700 W).

as-grown GaN surface. The results reveal that no etching products are left on the surface. Based on the XPS results, it can be concluded that a sufficiently high temperature is an essential factor for the volatilization of the etching products.

Fig. 4(a) shows the surface morphology of the GaN surface after PASE of 500 W. No obvious etching effect can be observed on the surface under RF power of 500 W. Microstructures are identified to be the deposition of etching products, while surface features on the as-grown surface such as hillocks could still be observed. The XPS results have confirmed that etching occurs but the etching products cannot escape from the surface. When RF power is increased to 600 W, etching pits are formed on the surface, as shown in Fig. 4(b). The shape of etching pits is

Table 2
Summary of the Ga3d XPS spectra and details of the components, peak position, FWHM, and ratio of the intensity of Ga-O and Ga-N peak.

	Components	Peak Position (eV)	FWHM (eV)	$\frac{I_{Ga-O}}{I_{Ga-N}}$
As-grown	Ga-N	20.3	1.2	0.240
	Ga-O	21.1	2	
	Metal Ga	17.6	2.7	
500 W	Ga-N	20.3	1.2	0.496
	Ga-O	21.1	2	
	Ga-F	23.1	2.5	
	Ga…H-F	19.3	1.8	
700 W	Ga-N	20.3	1.2	0.272
	Ga-O	21.1	2	
	Metal Ga	17.6	2.7	

close to semi-spherical. Under this condition, the etching initializes at some points on the surface with highly reactive dangling bonds. The etching rate is similar in every orientation, following the isotropic etching mode. It is revealed that the etching product has higher volatility and could volatile from the surface under this RF power and the corresponding temperature. When the RF power increases to 700 W, the hexagonal pyramid-shaped etching pits are formed on the surface, as shown in Fig. 4(c). In this etching mode, the etching begins to exhibit selectivity and preferentially occurred along the dislocation. While the horizontal etching rate V_h is relatively low to the etching rate along the dislocation V_d. As the RF power increases to 800 W, the etching pits become shallower and the bottom surfaces of the etching pits develop to be flat, which indicates a higher ratio of V_h to V_d, as shown in Fig. 4(d). Under the RF power of 900 W, the surface is very flat without any etching pits, signifying a fairly high ratio of V_h to V_z and V_d, as shown in Fig. 4(e). When the RF power is further increased to 1000 W, the major of the GaN surface maintains flat, as shown in Fig. 4(f).

During the PASE process, the temperature evolution of the GaN surface was measured by an infrared thermometer, as shown in Fig. 4(g). The RF power of PASE was fixed at 1000 W. The ICP torch acts as a heat source so that the surface temperature of GaN rises sharply in the initial stage. After about 10 s, when the sample surface temperature reaches a certain value, the heat absorption and heat dissipation on the sample surface are close to equilibrium, and the temperature keeps rising slowly. After 120 s, as the RF power is turned off, the plasma is unsustainable and the surface temperature drops rapidly, approaching the ambient temperature after about 8 min.

From the above discussion, we have confirmed that high RF power results in high temperature and high concentration of radicals. The most important operating parameter for achieving PASE is the surface temperature. Only when the temperature is high enough could the etching products volatilize from the surface entirely. Above all, the realization of surface flattening is mainly determined by the surface temperature. The ratio of horizontal etching rate to vertical etching rate increases with the temperature, which determines the etching mode and further surface morphology.

The surface roughnesses of the samples from the same wafer subjected to PASE for different durations were measured by SWLI. The detection area of SWLI was 400 × 40 0 μm. Fig. 5(a) shows the surface roughness evolution of the GaN surface during PASE under an RF power of 900 W. The initial GaN surface was lapped for 30 s with a roughness of *Sa* 308.5 nm, as shown in Fig. 5(b). At the initial stage of PASE, only etching pits are generated on the surface due to the insufficient reaction temperature, resulting in less improvement on the surface roughness. After 10 s, the GaN surface temperature is above the threshold where PASE can be achieved, and the surface roughness starts to decrease rapidly. With the progress of the reaction, the ratio of the lateral etching rate to the longitudinal etching rate increases. The etching pits gradually become shallower and connect with each other, and the roughness decreases steadily. The surface roughness is decreased to *Sa* 2.48 nm after

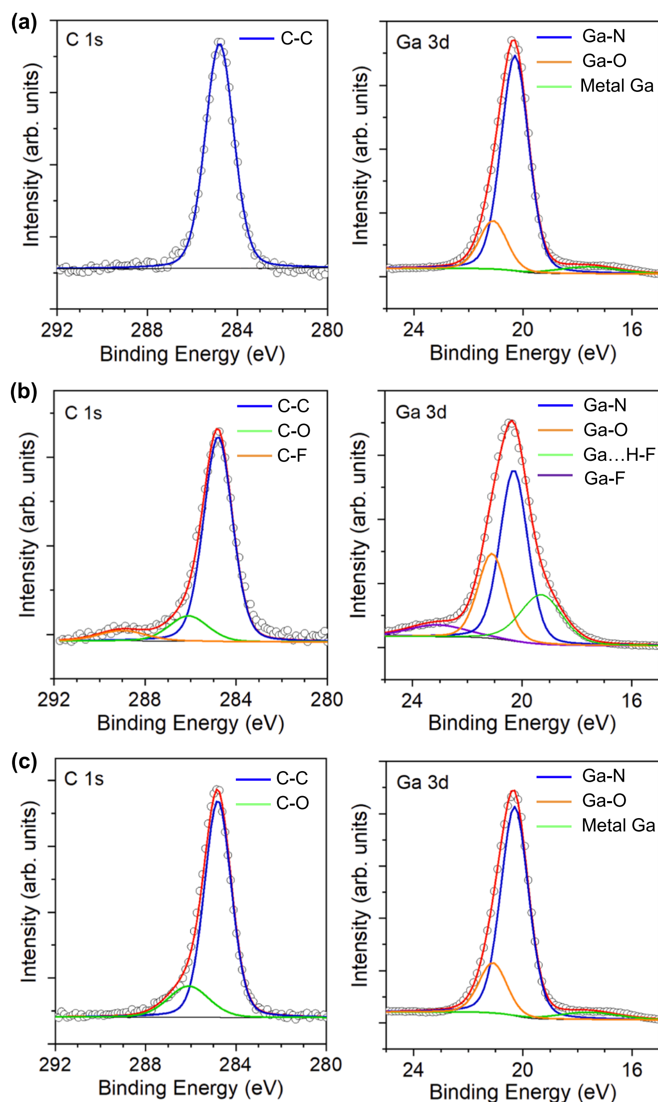

Fig. 3. Core-level XPS spectra of (a) as-grown sample: Ga3d and C1s; (b) sample after PASE with an RF power of 500 W: Ga3d and C1s; (c) sample after PASE with an RF power of 700 W: Ga3d and C1s.

2 min of PASE, as shown in Fig. 5(c).

The surface roughnesses at different scales were compared through SWLI and AFM measurements. The detection area of AFM was 10 × 1 0 μm. Fig. 5(d) and 5(e) show the AFM images and surface roughnesses of the GaN surface before and after PASE. The lapped surface is rough with cracks and pits with a surface roughness of *Sa* 135.8 nm. After 2 min of PASE, the surface roughness drops to *Sa* 2.68 nm. Before PASE, the SWLI results exhibit additional waviness information compared to the AFM results. After PASE, the surface roughnesses at different scales do not show a significant difference, proving that both the waviness and roughness of the surface can both be significantly reduced through PASE.

3.2. Material removal rate of the PASE

Before and after PASE, the sample weight was measured using a precision electronic balance with a resolution of 0.1 mg. The MRR of PASE of GaN can be calculated by the following equation:

$$MRR = \frac{\Delta m}{\rho \times S \times t}$$

Where Δm is the mass difference, S is the surface area, ρ is the density of GaN, t is the duration of PASE.

According to the Arrhenius equation, both the reaction temperature and the concentration of radicals have an impact on the MRR. Six sets of the experiment under different flow rates of CF_4 with a range of 10 sccm to 60 sccm were carried out, respectively. The RF power was fixed at 900 W. The intensity of the C_2 peak and the MRR of PASE in each set of the experiment were measured and summarized. Fig. 6(a) shows the relationship between the intensity of the C_2 peak and the MRR of PASE. It can be concluded that the MRR increases linearly with the concentration of F radicals.

Five sets of the experiment under different RF powers with a range of 600 W to 1000 W were also carried out, respectively. The flow rate of CF_4 was fixed at 60 sccm. The GaN surface temperature and the MRR in each set of the experiment were measured and summarized. The RF power can affect the MRR of the PASE through two factors. On one hand, free electrons gain more kinetic energy from the electromagnetic field with increasing RF power, which leads to an increase in surface temperature. On the other hand, the increase of RF power promotes the dissociation process of the CF_4 molecules, which leads to an increase in the concentration of reactive radicals.

The relationship between the RF power and the intensity of the C_2 peak has been concluded in Fig. 2(b). After excluding the influence of RF power on the intensity of the C_2 peak, the relationship between the GaN surface temperature and the MRR of PASE can be derived from the above results, as shown in Fig. 6(b). The maximum MRR can reach 93.01 μm/min under RF power of 1000 W, which is thousands of times higher than that of the conventional CMP process. Overall, the MRR of PASE increases linearly with increasing CF_4 flow rate. The MRR of PASE increases exponentially with increasing surface temperature, which is highly correlated to the Arrhenius equation. The relationship between reaction temperature and MRR can be fitted with the following equation:

$$MRR(T) = 3.51E7^{*}\exp^{\left(\frac{-15833.1}{T}\right)}$$

where T is the surface temperature.

The MRR of PASE was compared with other conventional polishing methods of GaN, as shown in Fig. 6(c). The surface area ratio between the 2-inch wafer and 10*10 mm sample was considered. The improvement of MRR is usually accompanied by the deterioration of surface roughness through conventional polishing methods using abrasives. Under the premise of achieving approximate surface roughness, the MRR of PASE is around three orders higher than that of MP and CMP processes.

In conclusion, the MRR of the PASE of GaN is determined by the reaction temperature and the concentration of radicals simultaneously. The above results further verify that PASE is a chemical-based etching process. The MRR of PASE of GaN can reach up to 93.01 μm/min, which is highly efficient. Even under conditions where PASE cannot be achieved, the material removal can also reach tens of microns. This means that all regions on the surface can be rapidly etched by the plasma, but dislocation regions on the surface will always be preferentially etched. The surface morphology will not get changed with time after the characteristics of the plasma reach a stable state. Since the dislocation has a higher reaction activity compared to the SE-atoms, etching pits will always exist on the surface. Only when the reaction temperature reaches above the threshold which leads to a higher etching rate of SE-atoms, could the surface planarization be realized.

3.3. Surface morphology evolution during PASE

Fig. 7 shows the SEM images and corresponding schematics of the GaN surface morphology evolution during the PASE process. As shown in Fig. 7(a), the as-grown surface is very rough with many hillocks [40,41]. In the initial stage of PASE, the topmost part of hillocks has a

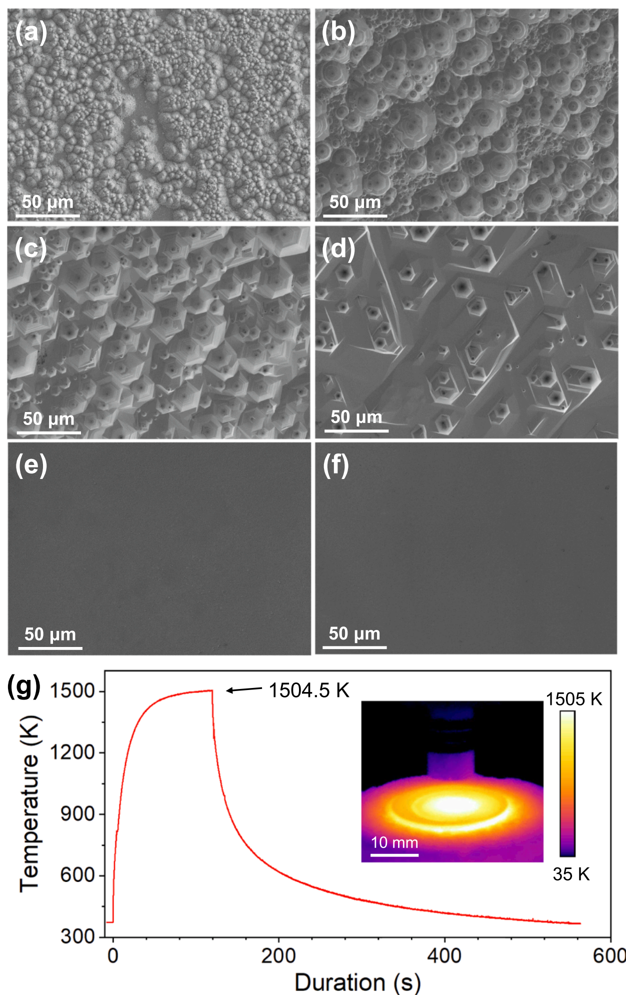

Fig. 4. (a-f) Surface morphology of GaN after PASE under different RF powers: (a) 500 W; (b) 600 W; (c) 700 W; (d) 800 W; (e) 900 W; (f) 1000 W. (g) Surface temperature evolution during PASE under RF power of 1000 W.

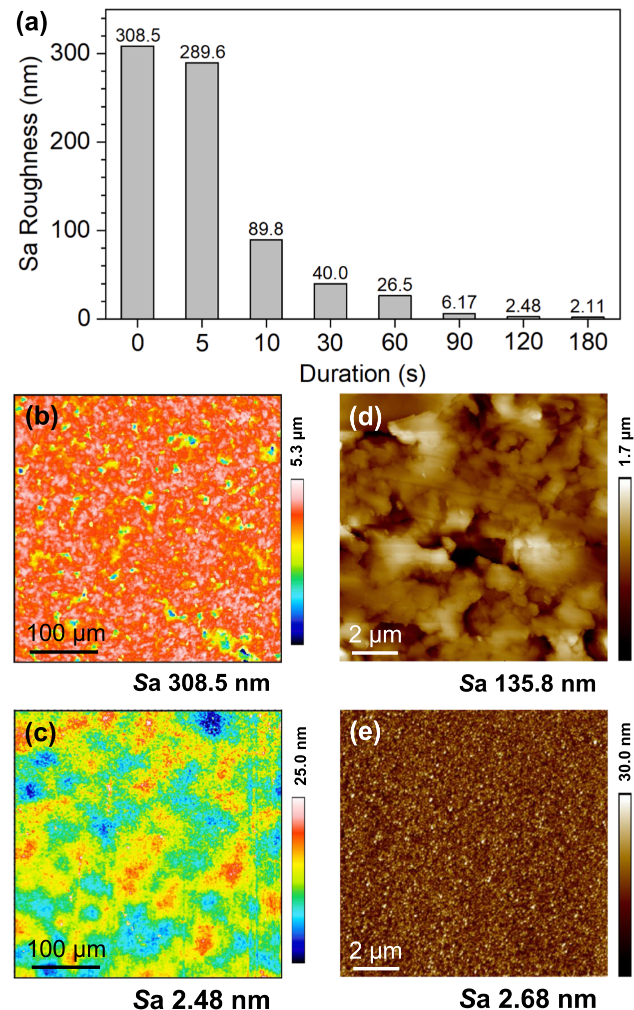

Fig. 5. (a) Surface roughness evolution of GaN during PASE measured by SWLI; (b) and (c) SWLI images of GaN surface morphology before and after PASE (400 × 400 μm); (d) and (e) AFM images of GaN surface morphology before and after PASE (10 × 10 μm).

lower reaction activation energy and is prone to be etched. Meanwhile, the etching pits can be observed on the surface where highly reactive dangling bonds exist, as shown in Fig. 7(b). Fig. 7(c) shows that the etching pits then become larger and shallower, and expand and overlap to form larger etching platforms. In this stage, the GaN surface temperature increases and results in a larger ratio of the lateral etching rate to the vertical etching rate. With the further increase in surface temperature, the horizontal etching rate is much higher than the vertical etching rate. The PASE mode has been realized in this stage and the surface becomes relatively flat, as shown in Fig. 7(d). As the duration of PASE continues to increase, the surface morphology does not show an obvious change and remains flat in PASE mode.

3.4. Surface thermal oxidation and its suppression after PASE

After a two-minute PASE process, the surface roughness of the GaN wafer drops from *Sa* 135.8 nm to *Sa* 2.68 nm. The surface oxide structure formed on the GaN surface after the PASE process is considered to be the main factor leading to the deterioration of the surface roughness.

To determine the chemical composition and morphology of the surface oxide, and the crystallographic structure of the GaN subsurface, scanning transmission electron microscopy (STEM) and EDX mapping were carried out. The TEM sample was prepared from the PASE-processed GaN surface by focused ion beam (FIB) milling and thinned to about 100 nm, as shown in Fig. 8(a). Fig. 8(b) shows a magnified cross-sectional STEM image of the outermost and near-surface regions of the GaN sample after PASE. The chemical composition of this region measured by EDX mapping is shown in Fig. 8(c). The top layer is a platinum (Pt) protective layer deposited by electron beam and ion beam with a low current, to prevent the sample from being damaged by ion milling. Below the Pt protective layer is the surface oxide layer. The shape of the surface oxide is approximately triangular from a cross-sectional view, and its height is measured to be around 60–70 nm. The bottom part is the GaN substrate, and the interface between the oxide layer and the GaN substrate is relatively flat. Excluding the growth of oxides, the surface can achieve the theoretical limit of surface roughness, which conforms to the principle of PASE. Fig. 8(d) shows a magnified STEM image of the surface oxide region just above the oxide/substrate interface. Its corresponding FFT pattern shown in the inset reveals that the gallium oxide has a regular crystal structure. Different from the thin, amorphous, and uniform surface oxide formed in air ambient, the oxide formed by thermal oxidation is crystalline with a rough surface [42–44]. Thermal oxidation of GaN occurs at temperatures above 800 centigrade in O_2 ambient [45]. It is revealed that the surface temperature is high enough after PASE to form a crystalline oxide layer on the surface, as shown in Fig. 4(g). Fig. 8(e) shows the region of the GaN substrate just below the interface and corresponding FFT. A typical diffraction pattern of GaN is observed [46]. Fig. 8(f) shows the magnified STEM image of the GaN substrate that the crystal

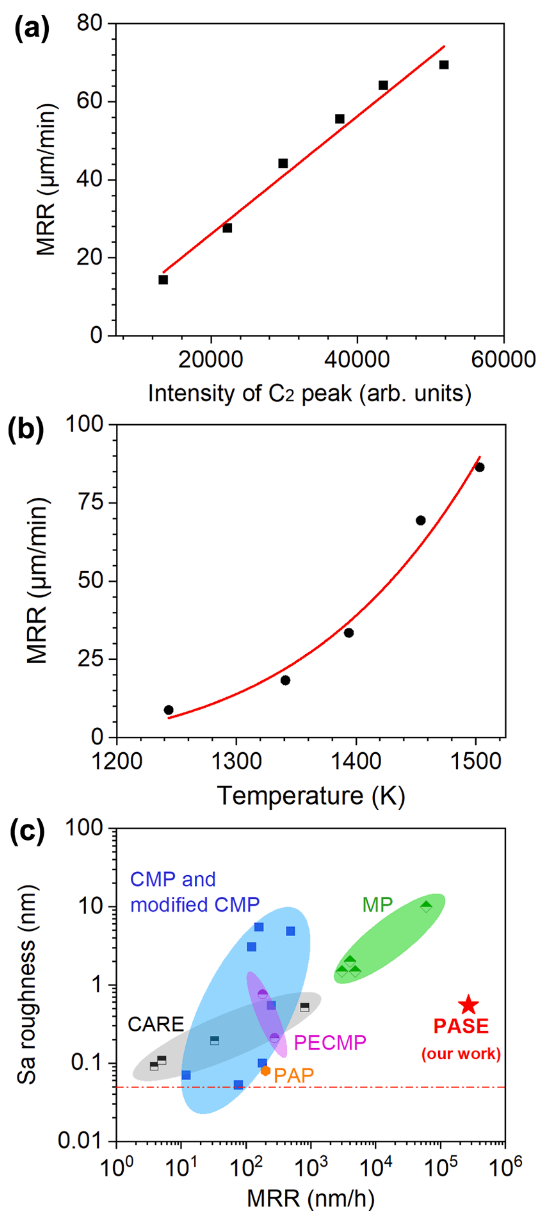

Fig. 6. (a) Relationship between MRR of PASE and the concentration of F radicals; (b) Relationship between MRR of PASE and the GaN surface temperature; (c) Comparison of PASE and other polishing methods.

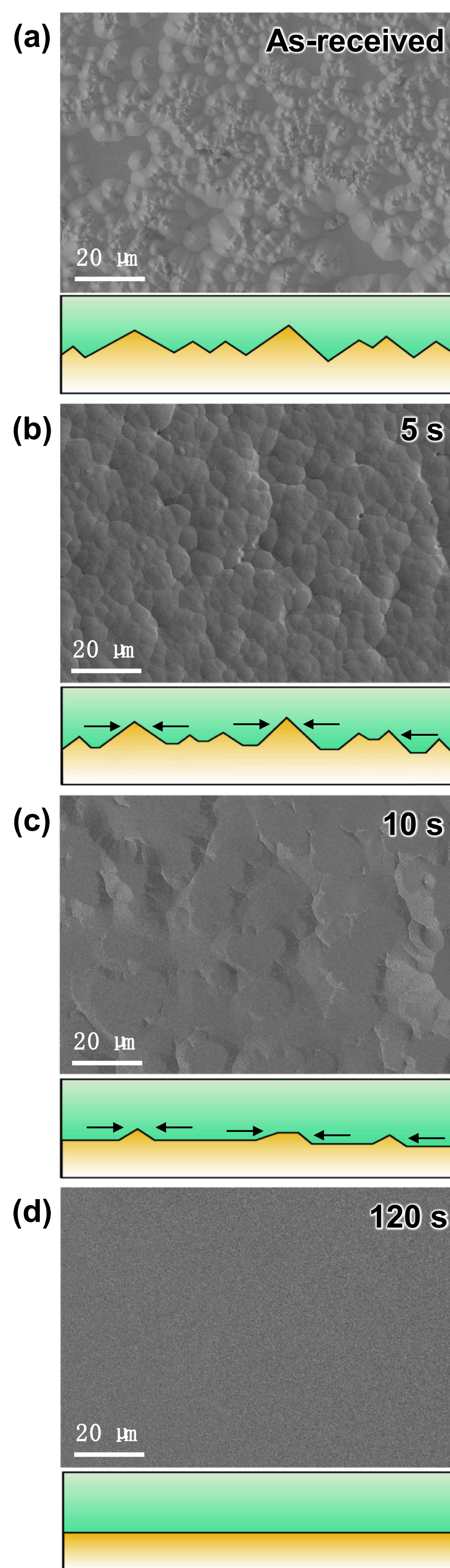

Fig. 7. SEM images and corresponding schematics of surface morphology of the GaN after PASE under different durations of PASE: (a) As-grown surface; (b) Generation of etching pits; (c) Expansion of etching pits; (d) Realization of surface planarization.

structure is regular without any defects or vacancies. The results indicate that PASE will not induce microcracks and amorphous phase to the GaN.

It can be concluded that the surface is mainly deteriorated by the uneven growth of surface oxide after PASE. To achieve a smoother surface and reduce the thickness of the oxide layer, the thermal oxidation process needs to be suppressed. High temperature and oxygen in the environment are the main causes of thermal oxidation. Since high temperature is an essential prerequisite in realizing the PASE of GaN, it is hard to inhibit thermal oxidation after PASE from the perspective of lowering the temperature during PASE. Hence, we employed a torch-down method to suppress thermal oxidation. After PASE, we first turned off the RF power and stopped the injection of CF_4. Immediately afterwards, we reduced the stand-off distance immediately until the torch could fully enclose the sample, as shown in Fig. 9(a). Continuous argon flow was then fed for 2 min to bring down the surface temperature below the threshold of thermal oxidation. Through this method, an argon atmosphere is formed on the sample surface and inhibits the oxygen from outside. In addition, the lower-temperature argon flow can reduce the surface temperature through thermal convection.

The surface morphology of the sample prepared by the torch-down method was examined by AFM, as shown in Fig. 9(b). The surface

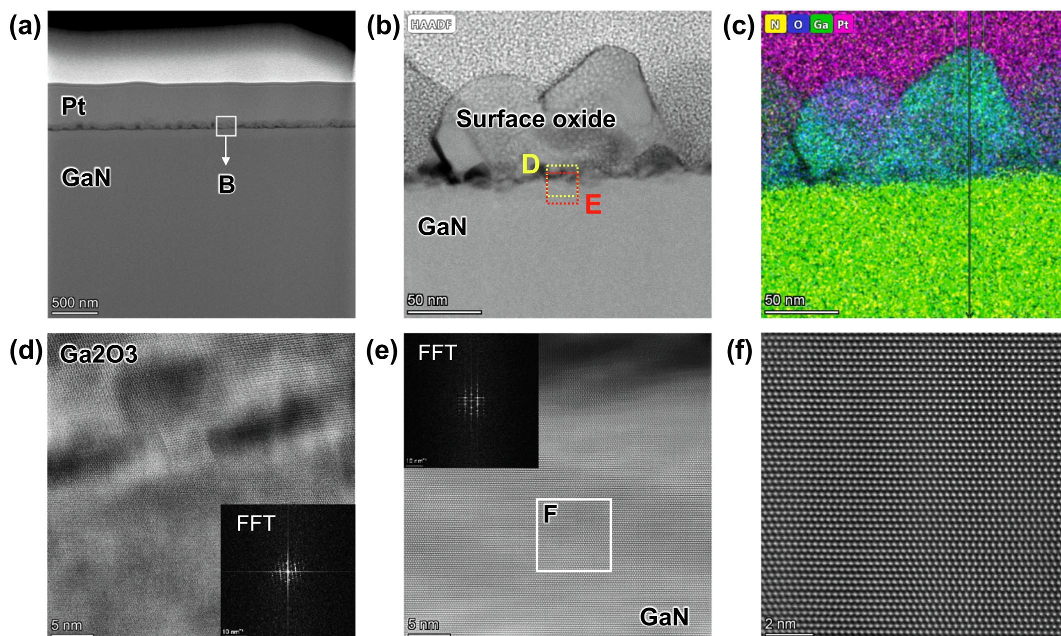

Fig. 8. (a) Cross-sectional STEM image of GaN prepared by FIB milling; (b) STEM image of the interface between GaN substrate and oxide layer; (c) EDX elemental mapping of the interface between GaN substrate and oxide layer; (d) Magnified STEM image of Ga2O3 and its corresponding FFT; (e) Magnified STEM image of GaN and its corresponding FFT; (f) High-resolution STEM image of GaN subsurface after PASE.

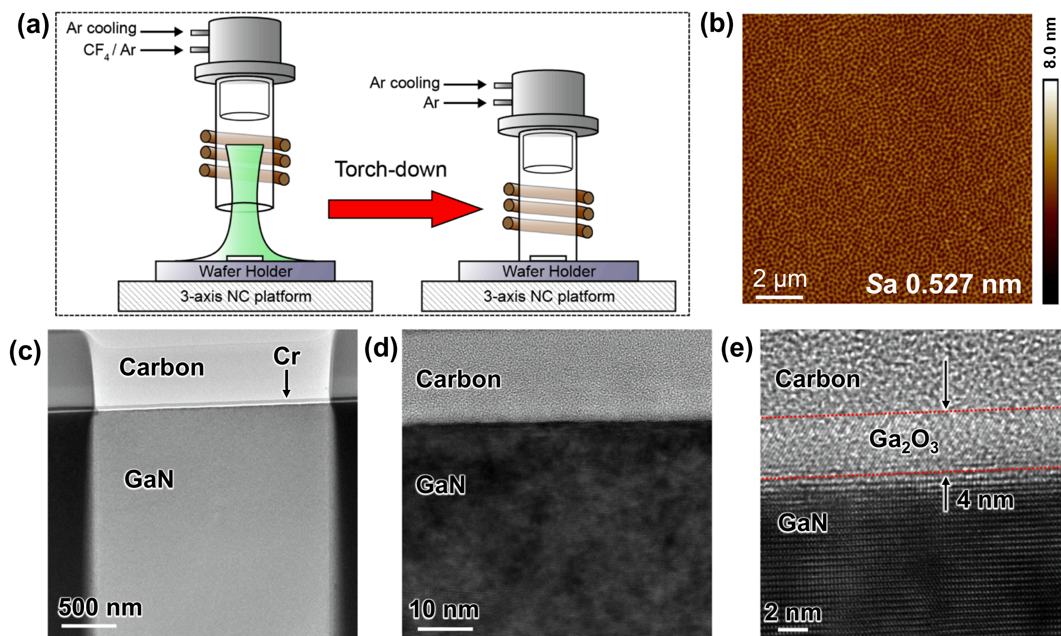

Fig. 9. (a) Schematic diagram of torch-down method for inhibiting thermal oxidation; (b) AFM image of the GaN surface after PASE and subsequent torch-down method; (c) Cross-sectional TEM image of GaN sample prepared by FIB milling; (d) Magnified TEM image of GaN topmost surface; (e) High-resolution TEM image of the interface between GaN substrate and oxide layer.

roughness is decreased to *Sa* 0.55 nm, which is comparatively smaller than the surface without treatment. Fig. 9(c) shows the cross-sectional TEM image of the sample prepared by the torch-down method. Carbon and chromium are deposited on the sample surface to prevent ion beam damage. Fig. 9(d) shows the interface between the GaN substrate and the deposited carbon layer. No obvious nanostructure can be observed on the interface. The high-resolution TEM image of the sample is shown in Fig. 9(e). A uniform oxide layer with a thickness of around 4 nm is formed on the topmost surface. The interface between the oxide layer and the GaN substrate is also very flat. The thickness of the thermal oxide is close to that of the natural oxide and will be easier to be removed by the subsequent CMP process.

4. Conclusion

PASE was conducted to realize the highly efficient surface planarization of GaN. The mechanism of PASE of GaN, the decisive operating parameters, and the etching characteristics were discussed. The following conclusions can be drawn from this study:

Non-toxic reaction gas CF_4 was utilized for the PASE of GaN. By using atmospheric inductively coupled plasma with high temperature and high concentration of radicals, etching products of GaN have good volatility and will not remain on the surface.
Temperature is a key factor in determining the PASE etching mode of GaN. As the temperature increases, the difference between the lateral and vertical etching rate becomes higher. The plasmas with high temperatures and sufficient reactive radicals have the potential to achieve surface polishing under proper conditions.
The crystal structure of the GaN subsurface is well-ordered without microcracks and amorphous phase, which indicates PASE is a non-destructive polishing method.
The surface roughness can drop from *Sa* 135.8 nm to *Sa* 2.68 nm after 2 min of PASE. Thermal oxidation is the main reason why surface roughness cannot be further reduced. A torch-down method can be conducted after PASE to suppress the thermal oxidation, and the roughness can be further decreased to *Sa* 0.527 nm. The material removal rate can reach 93.01 μm/min on a 10 × 10 mm^2 GaN sample.

As a semi-finishing process, PASE can replace the grinding and lapping process in conventional wafer fabrication, which greatly reduces the time cost.

CRediT authorship contribution statement

Linfeng Zhang: Conceptualization, Methodology, Writing – original draft. **Bing Wu:** Investigation, Methodology. **Yi Zhang:** Methodology. **Hui Deng:** Conceptualization, Writing – review & editing.

Declaration of Competing Interest

The authors declare that they have no known competing financial interests or personal relationships that could have appeared to influence the work reported in this paper.

Data availability

Data will be made available on request.

Acknowledgment

This work is financially supported by the National Natural Science Foundation of China (Grant No. 52035009, 52005243), the Natural Science Foundation of Guangdong Province (2023A1515011461) and the Science, Technology and Innovation Commission of Shenzhen Municipality (JCYJ20200109141003910, JCYJ20210324120402007), Shenzhen, China. The author acknowledges the assistance of SUSTech Core Research Facilities.

References

[1] A.S.A. Fletcher, D. Nirmal, A survey of Gallium Nitride HEMT for RF and high power applications, Superlattice. Microst. 109 (2017) 519–537.
[2] M.H. Kane, N. Arefin, Gallium nitride (GaN) on silicon substrates for LEDs, in: Nitride Semiconductor Light-Emitting Diodes (LEDs), 2018, pp. 79-121.
[3] H. Aida, H. Takeda, T. Doi, Analysis of mechanically induced subsurface damage and its removal by chemical mechanical polishing for gallium nitride substrate, Precis. Eng. 67 (2021) 350–358.
[4] J. Wang, T. Wang, G. Pan, X. Lu, Effects of catalyst concentration and ultraviolet intensity on chemical mechanical polishing of GaN, Appl. Surf. Sci. 378 (2016) 130–135.
[5] X. Shi, C. Zou, G. Pan, H. Gong, L. Xu, Y. Zhou, Atomically smooth gallium nitride surface prepared by chemical-mechanical polishing with $S_2O_8^{2-}$-Fe^{2+} based slurry, Tribol. Int. 110 (2017) 441–450.
[6] Y. Zhu, X. Niu, Z. Hou, Y. Zhang, Y. Shi, R. Wang, Effect and mechanism of oxidant on alkaline chemical mechanical polishing of gallium nitride thin films, Mater. Sci. Semicond. Process. 138 (2022), 106272.
[7] J. Murata, S. Sadakuni, T. Okamoto, A.N. Hattori, K. Yagi, Y. Sano, K. Arima, K. Yamauchi, Structural and chemical characteristics of atomically smooth GaN surfaces prepared by abrasive-free polishing with Pt catalyst, J. Cryst. Growth 349 (2012) 83–88.
[8] H. Kida, A. Isohashi, T. Inada, S. Matsuyama, Y. Sano, K. Yamauchi, High-efficiency Planarization of GaN Wefers by Catalyst-Referred Etching Employing Photoelectrochemical Oxdation, in: ICPT 2017; International Conference on Planarization/CMP Technology, 2017, pp. 1-4.
[9] Z. Dong, L. Ou, R. Kang, H. Hu, B. Zhang, D. Guo, K. Shi, Photoelectrochemical mechanical polishing method for n-type gallium nitride, CIRP Ann. 68 (2019) 205–208.
[10] L. Ou, S. Guo, Y. Zhe, Z. Dong, R. Kang, D. Guo, K. Shi, Polishing tool with phyllotactic distributed through-holes for photochemically combined mechanical polishing of N-type gallium nitride wafers, Precis. Eng. 66 (2020) 135–143.
[11] Y. Geng, Y. Yan, J. Wang, Y. Zhuang, Fabrication of Nanopatterns on Silicon Surface by Combining AFM-Based Scratching and RIE Methods, Nanomanufacturing and Metrology 1 (2018) 225–235.
[12] S.J. Pearton, R.J. Shul, Chapter 8 - Plasma etching of GaN and related materials, in: H. Singh Nalwa (Ed.), Handbook of Thin Films, Academic Press, Burlington, 2002, pp. 409–453.
[13] Z.Z. Chen, Z.X. Qin, Y.Z. Tong, X.M. Ding, X.D. Hu, T.J. Yu, Z.J. Yang, G.Y. Zhang, Etching damage and its recovery in n-GaN by reactive ion etching, Phys. B Condens. Matter 334 (2003) 188–192.
[14] R. Kawakami, T. Inaoka, Effect of argon plasma etching damage on electrical characteristics of gallium nitride, Vacuum 83 (2008) 490–492.
[15] F. Le Roux, N. Possémé, P. Burtin, P. Gergaud, V. Delaye, Characterization of AlGaN/GaN degradations during plasma etching for power devices, Microelectron. Eng. 249 (2021), 111619.
[16] C. Tendero, C. Tixier, P. Tristant, J. Desmaison, P. Leprince, Atmospheric pressure plasmas: A review, Spectrochim. Acta B At. Spectrosc. 61 (2006) 2–30.
[17] Y. Zhang, L. Zhang, K. Chen, D. Liu, D. Lu, H. Deng, Rapid subsurface damage detection of SiC using inductivity coupled plasma, International Journal of Extreme Manufacturing 3 (2021), 035202.
[18] K. Yamamura, Y. Yamamoto, H. Deng, Preliminary Study on Chemical Figuring and Finishing of Sintered SiC Substrate Using Atmospheric Pressure Plasma, Procedia CIRP 3 (2012) 335–339.
[19] Y. Mori, K. Yamauchi, K. Yamamura, Y. Sano, Development of plasma chemical vaporization machining, Rev. Sci. Instrum. 71 (2000) 4627–4632.
[20] Y. Mori, K. Yamamura, K. Yamauchi, K. Yoshii, T. Kataoka, K. Endo, K. Inagaki, H. Kakiuchi, Plasma CVM (Chemical Vaporization Machining): – A Chemical Machining Method With Equal Performances to Conventional Mechanical Methods from the Sense of Removal Rates and Spatial Resolutions –, in: N. Ikawa, S. Shimada, T. Moriwaki, P.A. McKeown, R.C. Spragg (Eds.), international Progress in Precision Engineering, Newnes, 1993, pp. 78–87.
[21] Y. Nakahama, N. Kanetsuki, T. Funaki, M. Kadono, Y. Sano, K. Yamamura, K. Endo, Y. Mori, Etching characteristics of GaN by plasma chemical vaporization machining, Surf. Interface Anal. 40 (2008) 1566–1570.
[22] C. Fanara, P. Shore, J.R. Nicholls, N. Lyford, J. Kelley, J. Carr, P. Sommer, A New Reactive Atom Plasma Technology (RAPT) for Precision Machining: the Etching of ULE® Surfaces, Adv. Eng. Mater. 8 (2006) 933–939.
[23] P.S. Fiske, Y. Verma, A. Chang, N. Lyford, J. Kelley, P. Sommer, N. Li, K. Pang, G. Gardopee, T. Kyler, J. Berrett, Reactive Atom Plasma Processing for Lightweight SiC Mirrors, in: Frontiers in Optics, Optica Publishing Group, Rochester, New York, 2006, pp. OFMB1.
[24] M. Castelli, R. Jourdain, P. Morantz, P. Shore, Rapid optical surface figuring using reactive atom plasma, Precis. Eng. 36 (2012) 467–476.
[25] H. Deng, K. Endo, K. Yamamura, Plasma-assisted polishing of gallium nitride to obtain a pit-free and atomically flat surface, CIRP Ann. 64 (2015) 531–534.
[26] Y.C. Lin, S.J. Chang, Y.K. Su, S.C. Shei, S.J. Hsu, Inductively coupled plasma etching of GaN using Cl_2/He gases, Mater. Sci. Eng. B 98 (2003) 60–64.
[27] D.S. Rawal, H. Arora, V.R. Agarwal, S. Vinayak, A. Kapoor, B.K. Sehgal, R. Muralidharan, D. Saha, H.K. Malik, GaN etch rate and surface roughness evolution in Cl_2/Ar based inductively coupled plasma etching, Thin Solid Films 520 (2012) 7212–7218.
[28] S. Zhou, B. Cao, S. Liu, Dry etching characteristics of GaN using Cl_2/BCl_3 inductively coupled plasmas, Appl. Surf. Sci. 257 (2010) 905–910.
[29] H.S. Kim, G.Y. Yeom, J.W. Lee, T.I. Kim, A study of GaN etch mechanisms using inductively coupled Cl_2/Ar plasmas, Thin Solid Films 341 (1999) 180–183.
[30] R. Kawakami, M. Niibe, Y. Nakano, S.-I. Yanagiya, Y. Yoshitani, C. Azuma, T. Mukai, Effects of ultraviolet wavelength and intensity on AlGaN thin film surfaces irradiated simultaneously with CF_4 plasma and ultraviolet, Vacuum 159 (2019) 45–50.
[31] R. Kawakami, M. Niibe, Y. Nakano, T. Shirahama, S. Hirai, T. Mukai, Comparison between AlGaN surfaces etched by carbon tetrafluoride and argon plasmas: Effect of the fluorine impurities incorporated in the surface, Vacuum 119 (2015) 264–269.
[32] Z. Fang, Y. Zhang, R. Li, Y. Liang, H. Deng, An efficient approach for atomic-scale polishing of single-crystal silicon via plasma-based atom-selective etching, Int J Mach Tool Manu 159 (2020), 103649.
[33] T. Inoue, M. Matsui, H. Takayanagi, K. Komurasaki, Y. Arakawa, Effect of swirl flow on an atmospheric inductively coupled plasma supersonic jet, Vacuum 80 (2006) 1174–1178.
[34] H. Zhou, A. Bennett, M. Castelli, R. Jourdain, J. Guo, N. Yu, Design of a motorised plasma delivery system for ultra-precision large optical fabrication, International Journal of Extreme Manufacturing 2 (2020), 045301.
[35] A. Shen, Y. Zou, Q. Wang, R.A.W. Dryfe, X. Huang, S. Dou, L. Dai, S. Wang, Oxygen Reduction Reaction in a Droplet on Graphite: Direct Evidence that the Edge Is More Active than the Basal Plane, Angew. Chem. Int. Ed. 53 (2014) 10804–10808.

[36] R. Sun, X. Yang, K. Watanabe, S. Miyazaki, T. Fukano, M. Kitada, K. Arima, K. Kawai, K. Yamamura, Etching Characteristics of Quartz Crystal Wafers Using Argon-Based Atmospheric Pressure CF4 Plasma Stabilized by Ethanol Addition, Nanomanufacturing and Metrology 2 (2019) 168–176.
[37] M. Grodzicki, J.G. Rousset, P. Ciechanowicz, E. Piskorska-Hommel, D. Hommel, XPS studies on the role of arsenic incorporated into GaN, Vacuum 167 (2019) 73–76.
[38] R. Huang, T. Liu, Y. Zhao, Y. Zhu, Z. Huang, F. Li, J. Liu, L. Zhang, S. Zhang, A. Dingsun, H. Yang, Angular dependent XPS study of surface band bending on Ga-polar n-GaN, Appl. Surf. Sci. 440 (2018) 637–642.
[39] L.Q. Zhang, C.H. Zhang, J. Gou, L.H. Han, Y.T. Yang, Y.M. Sun, Y.F. Jin, PL and XPS study of radiation damage created by various slow highly charged heavy ions on GaN epitaxial layers, Nucl. Instrum. Methods Phys. Res., Sect. B 269 (2011) 2835–2839.
[40] F. Oehler, T. Zhu, S. Rhode, M.J. Kappers, C.J. Humphreys, R.A. Oliver, Surface morphology of homoepitaxial c-plane GaN: Hillocks and ridges, J. Cryst. Growth 383 (2013) 12–18.
[41] K. Zhou, J. Liu, S. Zhang, Z. Li, M. Feng, D. Li, L. Zhang, F. Wang, J. Zhu, H. Yang, Hillock formation and suppression on c-plane homoepitaxial GaN Layers grown by metalorganic vapor phase epitaxy, J. Cryst. Growth 371 (2013) 7–10.
[42] Ł. Janicki, R. Korbutowicz, M. Rudziński, P.P. Michałowski, S. Złotnik, M. Grodzicki, S. Gorantla, J. Serafińczuk, D. Hommel, R. Kudrawiec, Thermal oxidation of [0001] GaN in water vapor compared with dry and wet oxidation: Oxide properties and impact on GaN, Appl. Surf. Sci. 598 (2022), 153872.
[43] S.K. Jain, P. Goel, U. Varshney, T. Garg, N. Aggarwal, S. Krishna, S. Singh, G. Gupta, Impact of thermal oxidation on the electrical transport and chemical & electronic structure of the GaN film grown on Si and sapphire substrates, Applied Surface Science Advances 5 (2021), 100106.
[44] Y. Zhou, C. Ahyi, T. Isaacs-Smith, M. Bozack, C.-C. Tin, J. Williams, M. Park, A.-J. Cheng, J.-H. Park, D.-J. Kim, D. Wang, E.A. Preble, A. Hanser, K. Evans, Formation, etching and electrical characterization of a thermally grown gallium oxide on the Ga-face of a bulk GaN substrate, Solid State Electron. 52 (2008) 756–764.
[45] P. Chen, R. Zhang, X.F. Xu, Z.Z. Chen, Y.G. Zhou, S.Y. Xie, Y. Shi, B. Shen, S.L. Gu, Z.C. Huang, J. Hu, Y.D. Zheng, Oxidation of Gallium Nitride Epilayers in Dry Oxygen, MRS Internet J. Nitride Semicond. Res. 5 (2000) 866–872.
[46] C. Li, Y. Piao, B. Meng, Y. Hu, L. Li, F. Zhang, Phase transition and plastic deformation mechanisms induced by self-rotating grinding of GaN single crystals, Int J Mach Tool Manu 172 (2022), 103827.